SCIENTIFIC REPORTS
nature research

OPEN

Low noise all-fiber amplification of a coherent supercontinuum at 2 μm and its limits imposed by polarization noise

Alexander M. Heidt[1]✉, Joanna Modupeh Hodasi[2], Anupamaa Rampur[3], Dirk-Mathys Spangenberg[1], Manuel Ryser[1], Mariusz Klimczak[3] & Thomas Feurer[1]

We report a low noise, broadband, ultrafast Thulium/Holmium co-doped all-fiber chirped pulse amplifier, seeded by an Erbium-fiber system spectrally broadened via coherent supercontinuum generation in an all-normal dispersion photonic crystal fiber. The amplifier supports a – 20 dB bandwidth of more than 300 nm and delivers high quality 66 fs pulses with more than 70 kW peak power directly from the output fiber. The total relative intensity noise (RIN) integrated from 10 Hz to 20 MHz is 0.07%, which to our knowledge is the lowest reported RIN for wideband ultrafast amplifiers operating at 2 μm to date. This is achieved by eliminating noise-sensitive anomalous dispersion nonlinear dynamics from the spectral broadening stage. In addition, we identify the origin of the remaining excess RIN as polarization modulational instability (PMI), and propose a route towards complete elimination of this excess noise. Hence, our work paves the way for a next generation of ultra-low noise frequency combs and ultrashort pulse sources in the 2 μm spectral region that rival or even outperform the excellent noise characteristics of Erbium-fiber technology.

Ultrashort pulse sources and frequency combs operating in the 2 μm spectral region have become indispensable tools for spectroscopy and precision metrology, as well as important stepping stones for the exploration of the molecular fingerprint region in the mid-infrared via nonlinear frequency conversion[1–5]. The application-driven requirements for such sources are constantly becoming more demanding, and include wide spectral bandwidth, ultra-low noise, and high robustness. Direct laser emission in the 2 μm wavelength regime is possible through Thulium (Tm)- or Holmium (Ho)-doped silica fiber lasers, which have been scaled to the kilowatt average power level even in ultrafast operation, but with limited spectral bandwidths[6]. Spectrally broadband sources, which take advantage of the very broad gain bandwidth provided by Tm- and Ho-ions[7–9], are often based on Tm- and Ho-doped fiber amplifiers seeded by modelocked Erbium (Er)-fiber systems, which are spectrally broadened to the 2 μm region via the generation of Raman-shifted solitons, four-wave mixing, or supercontinuum generation in the anomalous dispersion region of a highly nonlinear fiber (HNLF)[4,10–16]. In this way, the maturity, robustness, and excellent performance parameters of Er:fiber technology operating in the 1.55 μm window can be conveniently extended to longer wavelengths and are easily power-scaled.

However, this approach is susceptible to possible degradation of temporal coherence and excessive noise amplification due to the nonlinear processes involved in the spectral broadening in the HNLF. It is well known that the nonlinear dynamics in the anomalous dispersion regime suffer from high sensitivity to quantum noise, leading to white-noise fluctuations of amplitude and phase of the spectrally broadened seed signal usually associated with modulational instability (MI)[17–20]. Consequently, the noise performance of the 2 μm system is inherently degraded in comparison to the Er-fiber seed due the introduction of excess amplitude and phase noise at the nonlinear broadening stage, which is then further increased in the subsequent amplifier. The reported integrated root mean squared (rms) relative intensity noise (RIN) values of such systems operating at 2 μm are typically in the range 0.3–0.7%, which is about an order of magnitude higher than corresponding Er-fiber systems operating at 1.55 μm[4,10,12–14]. In fact, such white-noise-like RIN originating from the nonlinear processes in the

[1]Institute of Applied Physics, University of Bern, Sidlerstrasse 5, 3012 Bern, Switzerland. [2]Department of Physics, University of Ghana, Legon, Accra, Ghana. [3]Faculty of Physics, University of Warsaw, Pasteura 5, 02-093 Warsaw, Poland. ✉email: alexander.heidt@iap.unibe.ch

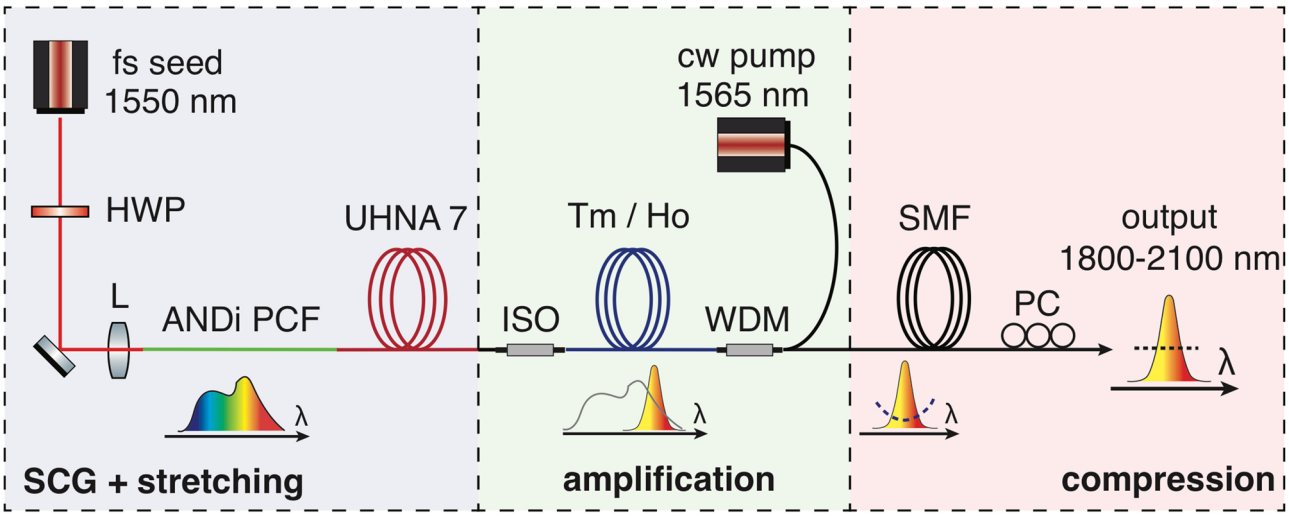

Figure 1. Layout of the fiber chirped pulse amplifier. The evolution of the spectrum is schematically illustrated below the fiber sections. Dashed lines in the spectrum symbolize spectral phase. *HWP* half-wave plate, *L* aspheric lens, *ISO* isolator, *WDM* wavelength division multiplexer, *PC* polarization controller.

spectral broadening stage has recently been identified as the major performance limiting factor in the further development of high power frequency comb sources at 2 µm[4,10].

Other system designs, which directly amplify modelocked oscillators at 2 µm, exploit nonlinear compression schemes such as soliton self-compression, which are based on anomalous dispersion nonlinear effects in the amplifier fibers or subsequent nonlinear fibers to reach comparable spectral bandwidths and pulse durations as the Er-fiber seeded systems. Hence, they are similarly susceptible to nonlinear noise amplification with reported integrated RIN values of $> 0.3\%$[21–23].

In this work we overcome these current limitations by completely eliminating noise-sensitive anomalous dispersion nonlinear dynamics from the spectral broadening stage. Instead, we employ an all-normal dispersion photonic crystal fiber (ANDi PCF) for coherent supercontinuum (SC) generation[24,25], which serves as the broadband coherent seed of a Tm/Ho amplifier. Normal dispersion nonlinear dynamics were recently reported to have a factor of 50 higher threshold for the onset of noise-driven decoherence compared to equivalent spectral broadening in the anomalous dispersion regime[26]. In addition, all-normal dispersion nonlinear processes also minimize the temporal jitter between different wavelength components[27], can exhibit lower RIN than the pump laser[28,29], and produce flat, smooth and stable spectra that can be compressed to high quality single-cycle pulses[30,31]. Hence, ANDi SC are ideally suited for the coherent seeding of ultra-low noise, broadband, ultrafast fiber amplifier systems. While carrier-envelope stabilized ANDi SC pulses were previously used for seeding of ultra-broadband optical parametric amplifiers[32], which were instrumental in enabling the first demonstrations of high harmonics generation and isolated attosecond pulses at high average power[33], this approach has so far not been applied to fiber optic systems.

We report a broadband, ultrafast Tm/Ho co-doped all-fiber chirped pulse amplifier, seeded by an Er-fiber system spectrally broadened in an ANDi PCF, supporting a − 20 dB bandwidth of more than 300 nm and delivering high quality 66 fs pulses with more than 70 kW peak power directly from the output fiber. This is amongst the shortest reported pulse durations for similar systems that do not use nonlinear post-compression schemes[10–13,15,16]. The total RIN integrated from 10 Hz to 20 MHz is 0.07%, which to our knowledge is the lowest reported RIN for wideband ultrafast amplifiers operating at 2 µm to date. The value further reduces to 0.03% if the more commonly quoted range up to 1 MHz is considered. In addition, we identify the origin of the remaining excess RIN as polarization modulational instability (PMI), and propose a route towards complete elimination of this excess noise. Hence, our work paves the way for a next generation of ultra-low noise frequency combs and ultrashort pulse sources in the 2 µm spectral region that rival or even outperform the excellent noise characteristics of Er-fiber technology.

Results

System design. The experimental setup is illustrated in Fig. 1. We employ a fiber chirped pulse amplifier (FCPA) scheme, consisting of a spectral broadening stage based on ANDi SC generation, followed by a dispersive pulse stretching and Tm/Ho co-doped fiber amplifier stage, and finally a fiberized pulse compression stage. While the Er-fiber seed laser pulses are free-space coupled to the ANDi PCF, the subsequent FCPA system is realised in an all-fiber configuration such that the amplified and compressed pulses are directly available at the fiber exit of the system.

The ANDi PCF was drawn in-house with a core diameter of 2.3 µm surrounded by a photonic crystal lattice realized in an all-solid design using two thermally compatible silicate glasses. Schott SF6 is used as core and lattice glass, Schott F2 for lattice inclusions and tube glass. More details of fiber design and production are given

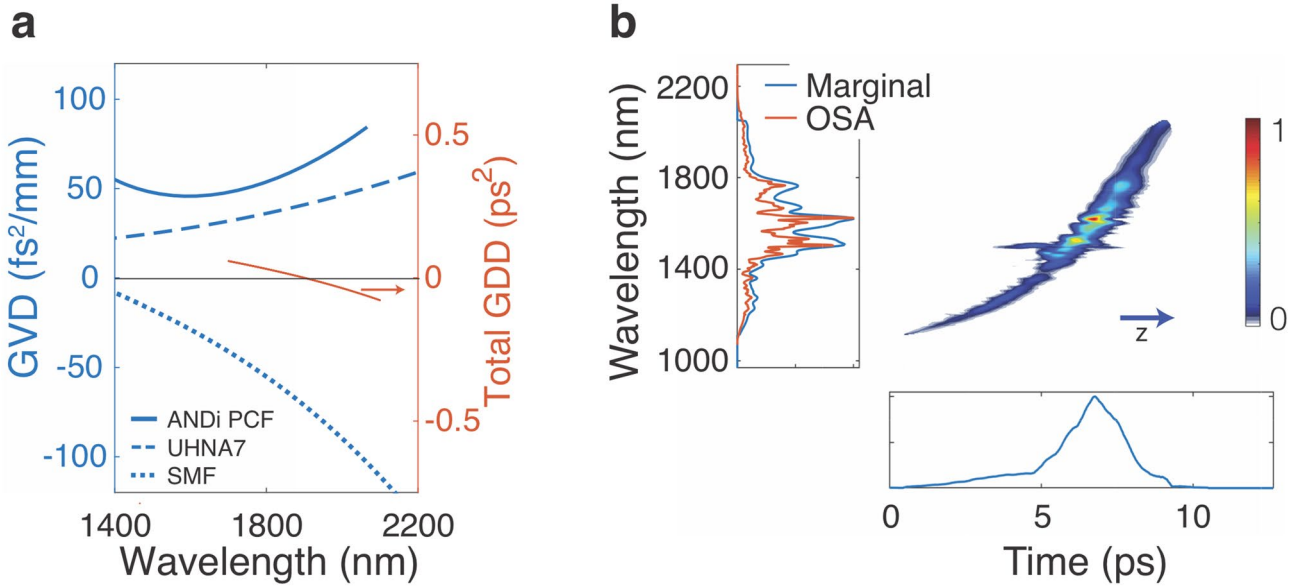

Figure 2. (**a**) Left axis (blue): Measured group velocity dispersion (GVD) of ANDi PCF, UHNA 7 and standard single mode fiber (SMF) (SM 2000, Thorlabs)[36,37]. Right axis (red): Total group delay dispersion (GDD) of the amplifier system, representing the uncompensated material dispersion at the exit of the system. (**b**) Projected axis spectrogram of the SC pulse in linear scale at the exit of 20 cm ANDi PCF under similar pumping conditions as used in the amplifier system, measured using time-domain ptychography based on a cross-correlation with the Er-fiber seed laser[35]. The correlation of the spectral marginal to an independently measured optical spectrum analyzer (OSA) trace validates the accuracy of the measurement. *z* indicates the propagation direction.

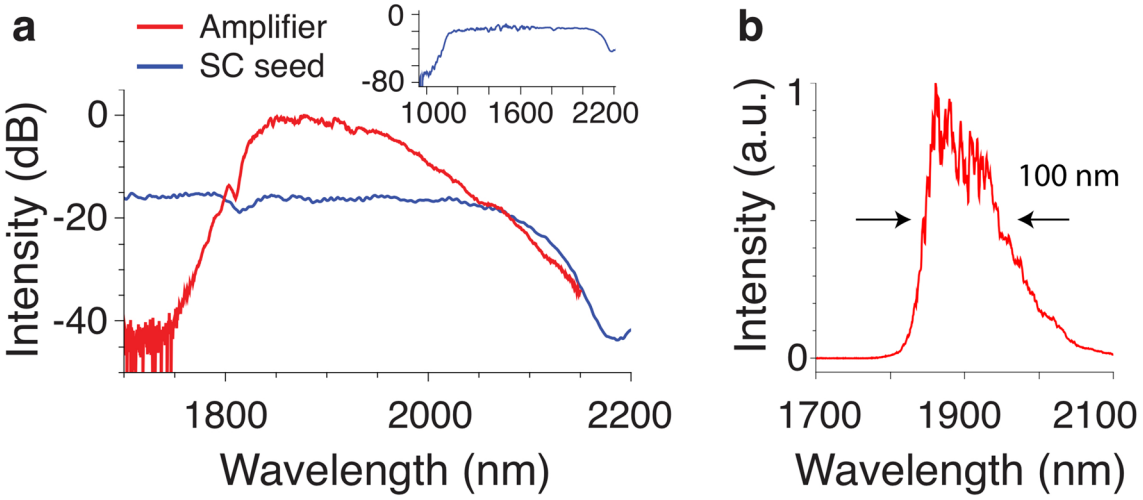

Figure 3. (**a**) Logarithmic spectra of SC seed pulse and amplifier (not to scale). The inset shows the complete spectrum of the spectrally broadened seed pulse. (**b**) Linear amplifier spectrum.

elsewhere[34]. The fiber provides high nonlinearity ($\gamma \approx 214$ (W km)$^{-1}$ at 1560 nm) and normal group velocity dispersion (GVD) over the entire wavelength region of interest, as shown in the measured GVD curve in Fig. 2a.

The seed pulses are provided by a commercial Er-fiber system, delivering 100 fs pulses with 80 MHz repetition rate at a central wavelength of 1560 nm. Coherent SC generation in the 20 cm long ANDi PCF is used to spectrally broaden the pulses sufficiently for seeding the entire gain bandwidth of the Tm/Ho amplifier in the 1750–2200 nm range. The coupling efficiency into the ANDi PCF is about 60%, and we found that a coupled peak power of 20 kW is sufficient for achieving a uniform seeding level of the entire Tm/Ho emission band. The corresponding SC spectrum at the exit of the ANDi PCF, shown in logarithmic scale in the inset of Fig. 3a, covers the wavelength range 1120–2150 nm at a − 20 dB level. Increasing the peak power of the seed pulses increases the SC bandwidth, while the spectral shape and power contained in the section coinciding with the Tm/Ho emission band remains relatively constant. Therefore, higher peak powers do not necessarily lead to a better seeding of the amplifier. Figure 2b shows a typical measured projected axes spectrogram of the SC pulse in linear

scale at the exit of the ANDi PCF under similar pumping conditions as used in the FCPA. The spectrogram was measured using time-domain ptychography based on a cross-correlation with the Er-fiber seed laser according to the procedure outlined in literature[35]. It is evident that the normal dispersion nonlinear processes, dominated by self-phase modulation and optical wave braking, preserve the temporal integrity of the SC pulse[26]. The chirp is predominantly linear at the long wavelength wing between 1750 and 2200 nm, i.e. the SC pulse is very well suited as a seed for the ultrafast Tm/Ho amplifier.

The SC pulses are further dispersively stretched in 6.8 m of UHNA 7 fiber (Nufern; core diameter 2.4 µm, 0.41 NA), which has normal dispersion in the Tm/Ho amplification window and is used to compensate the anomalous dispersion of the active and passive fibers of the subsequent amplifier system[37]. The measured GVD curve of this fiber is shown in Fig. 2a and compared to the GVD of the standard single-mode fiber (SMF) (SM 2000, Thorlabs) used as pigtail fiber of the passive components in the amplifier. Note that we did not measure the GVD of the active fiber used in our system, but based on previous reports we assume it to be similar to passive SMF[38]. The measured dispersion coefficients of UHNA 7 at 1900 nm ($\beta_2 = +41\text{fs}^2/\text{mm}$, $\beta_3 = -99\text{fs}^3/\text{mm}$) compensate not only second, but also the third order dispersion of SMF ($\beta_2 = -71\text{fs}^2/\text{mm}$, $\beta_3 = 330\text{fs}^3/\text{mm}$). This is an important requirement for achieving a high quality compressed pulse at the output of the system. Nevertheless, higher order material dispersion cannot be completely compensated in this all-fiber configuration, which is illustrated by the total group delay dispersion (GDD) of the amplifier system shown in Fig. 2a calculated by multiplying the GVD values of each fiber with the respective fiber lengths used in the system and taking the sum. This uncompensated material dispersion ultimately limits the obtainable pulse quality, as discussed below. UHNA 7 also acts as an efficient mode field adapter between ANDi PCF and SMF, because its small core with high NA efficiently collects the light exiting the PCF while the expansion of the core under fusion splicing can be used to minimize splice loss to SMF to < 0.2 dB. This allows seeding the subsequent amplifier with approx. 11 mW of average power contained in the relevant spectral range of 1750–2200 nm of the SC pulse.

The amplifier consists of 140 cm of Tm/Ho co-doped single-mode fiber (CorActive Th512; 9 µm core diameter, 0.16 NA, 150 dB/m core absorption at 790 nm), backward core-pumped via a wavelength-division multiplexer by an in-house built Erbium/Ytterbium (Er/Yb) co-doped single-mode fiber laser operating at 1560 nm. The length of the Tm/Ho doped fiber was optimized for maximum FWHM spectral bandwidth of the amplified signal by balancing the gain contributions of both types of active ions, which requires reabsorption of the Tm-ion emission to pump the Ho-ions[39]. Therefore, this length does not coincide with the length required for operation with highest optical-to-optical efficiency, which would be significantly shorter due to the high core absorption of the doped fiber. The pulses temporally compress during propagation in the amplifier due to the anomalous dispersion of the active and passive fibers, but it remains positively chirped with a pulse duration of about 6 ps at the exit of the amplifier. The final temporal recompression is then simply achieved by splicing an appropriate length (about 1.2 m) of SMF to the exit of the amplifier. Spurious reflections inside the amplifier are avoided by an in-line isolator at the amplifier input and an angle-cleaved fiber end-facet at the exit of the system. The polarization state is controlled by a half-wave plate at the input and a polarization controller near the output of the system. The seeding level is sufficient to operate the amplifier system near saturation, delivering a maximum of 0.5 W average output power at a pump power of 2 W. Further power scaling is limited by the small mode-field diameter of the current SMF compression fiber, which leads to excessive nonlinear effects and related pulse distortions at higher peak powers. However, this can be easily circumvented by using large-mode area compression fibers or external bulk compressors.

Spectral and temporal properties. The spectrum of the amplified signal in relation to the ANDi SC seed is shown in Fig. 3. The SC spectrum is sufficiently broad to coherently seed the entire gain bandwidth of the amplifier. As a consequence, incoherent amplified spontaneous emission (ASE) noise is not observed in the spectral domain, and is also not expected to build up temporally between pulses due to the high repetition rate (80 MHz) in comparison to the long ($\sim$ ms) excited state life time of Tm- and Ho-ions. The amplified signal has a central wavelength of 1900 nm, a − 20 dB spectral bandwidth of 310 nm (1798–2108 nm) and a FWHM of 100 nm. The Fourier-limited pulse duration is 45 fs, obtained from direct Fourier-transformation of the measured spectrum assuming flat spectral phase, resulting in a time-bandwidth product of TBP = 0.375. This indicates a pulse shape half way in between Gaussian and $sech^2$. Note that we do not apply any nonlinear pulse compression scheme in or after the amplifier, we observe only limited spectral broadening in the order of 15 nm (− 3 dB width) in the compression fiber. This is in contrast to previous demonstrations of similar amplifier systems using soliton self-compression, where nonlinearities and spectral broadening in the order of > 100 nm in the compression fiber play a significant role in obtaining sufficiently short pulses[4,23]. The minimization of nonlinearity in the amplifier and compression fiber, which exhibit anomalous dispersion, is an important feature to reduce nonlinear noise amplification in the amplifier system, as will be discussed below.

Figure 4a shows the measured autocorrelation (AC) trace of the system output with a FWHM of 98 fs. Applying the same deconvolution factor as obtained for the Fourier-limited pulse results in a pulse duration of 66 fs. The AC trace is exceptionally clean for an all-fiber CPA system; it does not exhibit any major side peaks, only the broadened base of the main peak indicates the presence of a pedestal. The absence of further side pulses was checked using an AC scan window of 150 ps as well as a fast photodiode and oscilloscope combination with 60 ps temporal resolution. The approximate deconvoluted pulse shape in Fig. 4b, obtained computationally by an iterative procedure reproducing the measured AC trace (see "Methods" section), reveals that 75% of the energy is contained in the central peak, with the remaining part mostly located in a low-level pedestal at the leading pulse edge. Using the measured pulse energy and duration and correcting for the energy content of the pedestal, we estimate the peak power of the output pulse to approximately 71 kW. The longer pulse duration in comparison to the Fourier-limit, also shown in Fig. 4b, and the occurrence of the pedestal can be attributed to

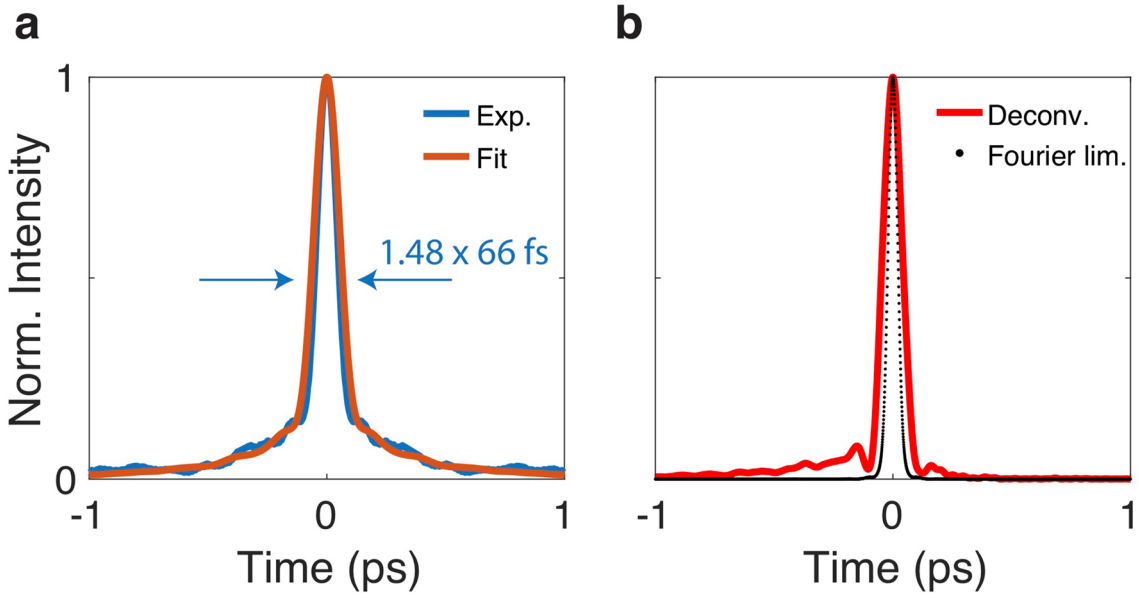

Figure 4. (**a**) Measured autocorrelation trace (Exp.) in comparison to the calculated trace (Fit) obtained by a procedure described in "Methods" section. (**b**) Deconvoluted pulse shape of the calculated trace (Deconv.) and Fourier limited pulse shape (Fourier lim.) obtained by direct Fourier transformation of the measured spectrum assuming flat spectral phase.

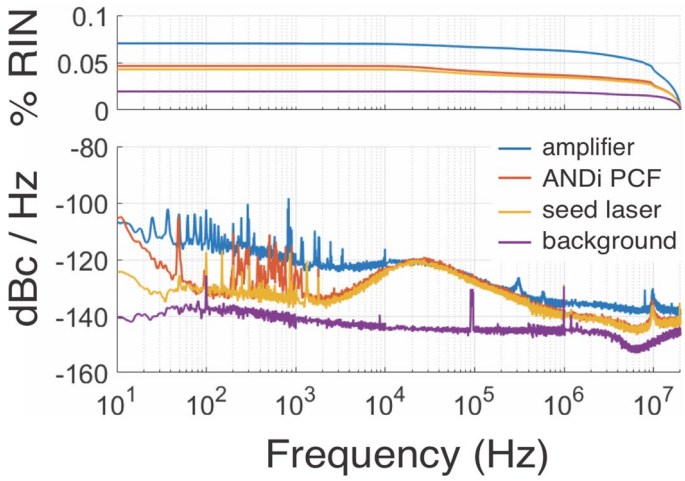

Figure 5. Amplitude noise measurements at different positions along the amplifier. The bottom shows the spectrally resolved amplitude noise in a range 10 Hz–20 MHz, while the top shows the total integrated RIN in percent. Shown are the noise of the Er-fiber seed laser before spectral broadening (yellow), the spectrally broadened seed after the ANDi PCF (red), and the amplified and compressed output of the Tm/Ho amplifier (blue). The noise floor of the measurement system is shown in purple.

the uncompensated higher order phase terms of the pulse, acquired as a combination of the residual material GDD shown in Fig. 2a and nonlinear phase changes introduced during SC generation and to a lesser extent also in the compression fiber. The fit of the autocorrelation trace returns residual third and fourth order phase of approximately $\Phi_3 = 3.5 \times 10^{-4}$ ps^3 and $\Phi_4 = -3.5 \times 10^{-5}$ ps^4, respectively. Minimizing the overall length of the system and using free-space compression could decrease the impact of uncompensated GDD and in consequence further improve the compressed pulse quality.

Amplitude noise measurements. Figure 5 shows the amplitude noise spectrum as well as the integrated rms RIN in the range 10 Hz–20 MHz measured at different positions along the amplifier. The RIN of the SC measured directly after the ANDi PCF (0.047%) is virtually identical to the RIN of the Er-fiber seed laser (0.045%), except for additional noise contributions in the frequency range 200 Hz–1 kHz. In order to facilitate other experiments, the Er-fiber system was located on a different optical table than the ANDi PCF and the rest

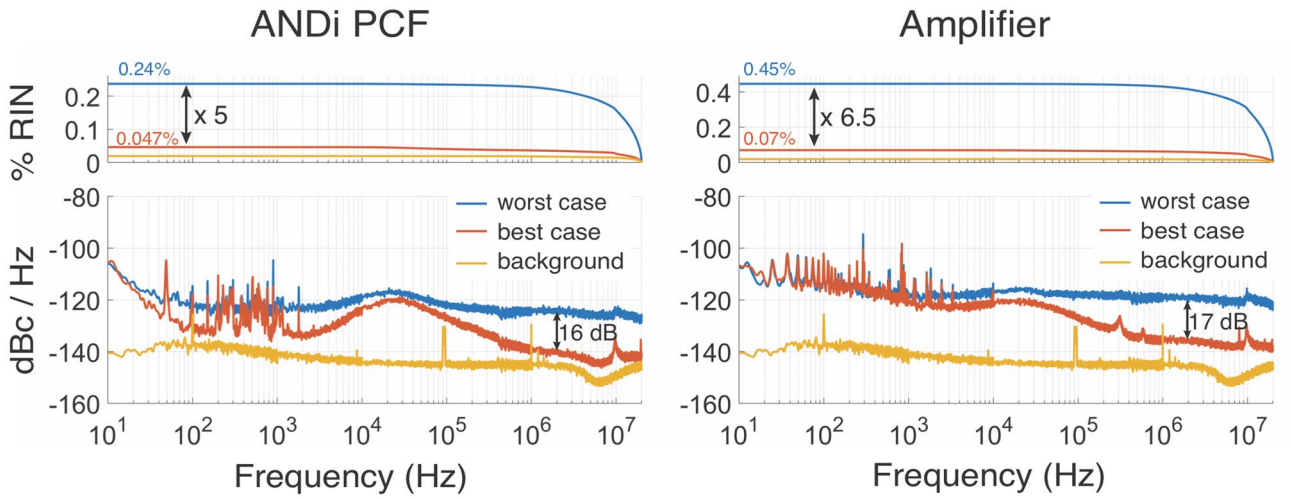

Figure 6. Dependence of the measured amplitude noise on the polarization state of the Er-fiber seed pulses coupled into the system. Best and worst case RIN measurements of the spectrally broadened seed after the ANDi PCF (left) and the amplifier output (right) obtained by rotating the half-wave plate at the input of the FCPA.

of the experiment, requiring a free space beam path of about 3 m length between the exit of the Er-fiber system and the coupling stage of the ANDi PCF. Hence, we attribute these additional low frequency noise components to vibrations caused by the laboratory environment resulting in beam pointing instabilities, which are translated to amplitude noise at the PCF input. After the amplifier, the total integrated RIN increases to 0.07%. If the more commonly quoted range up to 1 MHz is considered, the RIN of the amplifier output is 0.03%. Although this is an excellent value, we do observe an increase by a factor of about 1.5 compared to the RIN measured directly from the Er-fiber seed system, which is caused predominantly by an additional broadband noise component in the range 500 kHz–20 MHz. We attribute this excess high frequency noise to the nonlinear amplification of quantum noise using polarization modulation instability (PMI) (see Discussion). In the medium frequency range 20–300 kHz the amplifier RIN is dominated by the RIN of the Er-fiber seed system. We have determined that the excess noise of the amplifier in the low frequency range < 20 KHz originates from the continuous wave Er/Yb pump laser of the amplifier, more specifically from the electronic driver of the 980 nm semiconductor pump diodes employed in this laser. However, this low frequency noise has only negligible influence on the integrated RIN of the amplifier.

We observe a strong and sensitive dependence of the RIN on the input polarization state of the Er-fiber seed pulses coupled into the FCPA. This is illustrated in Fig. 6, both for the RIN measured directly after the ANDi PCF and after the amplifier. The input polarization of the seed pulses entering the ANDi PCF is varied by rotating the half-wave plate placed into the free-space beam path, and the best-case RIN measurements that were presented in Fig. 5 are compared to the observed worst-case RIN measurements obtained for a different setting of the half-wave plate. For the spectrally broadened seed after the ANDi PCF, in the worst-case setting the integrated RIN increases to 0.24% or a fivefold increase compared to the best-case setting. This increase is caused by an additional white-noise component that raises the entire amplitude noise spectrum by about 16 dB, which is most evident in the high frequency range. A similar behaviour is observed after the amplifier with a 6.5-fold increase of integrated RIN to 0.45% in the worst-case scenario. While the total RIN oscillates between these extrema in a complex pattern when rotating the input polarization, whose detailed analysis will be subject to future work, we observe only one stable global maximum and minimum setting. These extrema are very sensitive to the input polarization angle, with the RIN changing rapidly in a ± 1 degree range around them. In the worst-case settings we also observe fast fluctuations of the polarization state of the output pulses, which appear as additional broadband amplitude noise components when an additional polarizer is placed before the photodiode used for the RIN measurements[40]. In contrast, the best-case settings also show a stable polarization state. The optimum input polarization angle for low-noise operation changes with environmental conditions such as temperature or fiber coiling radius, which necessitates daily readjustment of the polarization settings. This observed polarization dependence of the RIN by far dominates over the impact of changing seeding or pump power levels of the amplifier, which only have marginal impact on the measured RIN levels.

Discussion

To our knowledge, the low amplifier RIN of 0.07% (10 Hz–20 MHz) and the small noise amplification factor of 1.5 represent the lowest values reported for wideband ultrafast amplifiers operating at 2 µm to date. Our amplifier system is designed in such a way that many of the traditional linear and nonlinear noise amplifying effects are effectively suppressed. Firstly, the normal dispersion nonlinear spectral broadening dynamics in the ANDI PCF exclude soliton dynamics and MI, which are associated with a loss of temporal coherence and corresponding white-noise amplitude and phase instabilities occurring in fibers with anomalous dispersion. Secondly, the chirped pulse amplification scheme and avoidance of nonlinear self-compression in the amplifier minimize

nonlinear noise-amplifying effects in the amplifier fibers, which do have anomalous dispersion at the operating wavelength. Thirdly, the broad spectral bandwidth of the ANDi SC coherently seeds the entire gain bandwidth of the Tm/Ho-doped amplifier fiber, which in combination with the high repetition rate effectively suppresses incoherent ASE noise. These measures explain the excellent performance of our amplifier in comparison to previous reports, where much larger RIN values and noise amplification factors were observed[4,10,12–14].

Nevertheless, we do observe highly polarization sensitive excess RIN both after the ANDi PCF and the amplifier largely caused by white-noise-like instabilities, which is especially evident at the high frequency range above 1 MHz. Such high-frequency white-noise is a typical signature of nonlinear amplification of quantum noise[19]. At the pump pulse durations we employ during SC generation ($\sim$ 100 fs), the only noise-amplifying nonlinear effect occurring in ANDi fibers is polarization modulational instability (PMI)[41,42]. In fact, the strong polarization dependence of the RIN, and the observed fast fluctuations of the polarization state of the output pulses in the worst-case settings, clearly identify PMI as source of the excess noise because the PMI gain is strongly sensitive to the relative orientation between input polarization state and the fiber's principal axes[42] . PMI leads to significant pulse-to-pulse fluctuations of amplitude, phase, and polarization state, and consequently leads to coherence degradation of SC pulses, in particular in weakly birefringent, non-polarization-maintaining fibers as we use in this system[41]. As unseeded PMI can be understood as the amplification of quantum or shot noise with random phase, it appears in the noise spectrum as white-noise instability[40]. This explains the experimentally observed RIN variations with rotation of the input polarization. Since we use non-polarization-maintaining fibers, the principal axes of the fibers are not well-defined and originate from an unintentional and weak birefringence induced by stress, e.g. from the drawing process or coiling on the optical table. Hence, the orientation of the principal axes may change with environmental conditions, as observed experimentally, negatively impacting the long-term stability of the system. While the ANDi PCF should be the main source of PMI noise due to the larger nonlinearity and high peak power of the propagating pulses, it is reasonable to assume additional PMI noise being generated in the amplifier as well. This is especially true if high peak powers are reached in the amplifier due to the use of nonlinear pulse shortening mechanisms, such as soliton self-compression, as was the case in recent reports[4,21,23]. In our system, the RIN measured directly after the Tm/Ho fiber is identical to the RIN measured at the system output, i.e. we do not observe any nonlinear noise amplification during compression.

It is important to note that PMI is not a phenomenon restricted to normal dispersion fibers, but also occurs in anomalous dispersion fibers in addition to the more well-known noise amplifying effects[42]. We would like to point out that PMI might be an important performance limiting factor contributing to the white-noise-like amplitude and phase instabilities observed in recent demonstrations of high power frequency combs at 2 µm, which were seeded by SC pumped in the anomalous dispersion regime and realized with non-polarization-maintaining fibers[4].

PMI in the SC generation process can be suppressed by employing only highly birefringent, polarization-maintaining (PM) fibers pumped along their principal axis[40–42]. In this case, the dominating noise-amplifying nonlinear effect in normal dispersion SC dynamics is the nonlinear coupling of stimulated Raman scattering and parametric four-wave mixing[26]. At the peak powers typically used for SC generation, this effect occurs only for pump pulse durations exceeding 1 ps and is effectively suppressed for shorter pump pulses[26]. Hence, our work paves the way for the construction of next generation ultra-low noise high power ultrashort pulse amplifiers and frequency combs practically free of excess noise by simply replacing all the fibers in our system with their corresponding PM version. Since PM ANDi fibers and corresponding SC sources are now available[43,44], this is a straightforward task. Indeed, our preliminary tests with a PM ANDi SC source and an all-PM chirped pulse amplification system indicate that the RIN after the amplifier is very close to the RIN of the Er-fiber seed system[45].

Methods

Deconvolution of the measured autocorrelation trace. For evaluation of the pulse quality we computationally reproduce the measured AC trace by adding third and fourth order spectral phase terms to the measured spectrum, taking the Fourier transform and calculating the AC trace of the corresponding pulse. The total uncompensated spectral phase of the pulse at the exit of the system stems from both the uncompensated material GDD of the FCPA system, shown in Fig. 2a, and from nonlinear phase changes introduced during SC generation and to a lesser extent also in the compression fiber. Hence, the measured material GDD is used to extract the starting values for the fit, which were determined to be $\Phi_{3M} = 6.4 \times 10^{-4}$ ps^3 and $\Phi_{4M} = -2.5 \times 10^{-6}$ ps^4. The total uncompensated third and fourth order spectral phases are then determined in an iterative procedure finding the best fit to the experimentally measured trace. A good fit is found for $\Phi_3 = 3.5 \times 10^{-4}$ ps^3 and $\Phi_4 = -3.5 \times 10^{-5}$ ps^4, which is compared to experimentally measured trace in Fig. 4a. While this calculation slightly overestimates the pulse duration, the shape of the AC trace is well reproduced.

Relative intensity noise measurements. The measurements were conducted according to the standards outlined in literature[46]. The amplitude noise was analyzed by an amplified photodiode (Thorlabs PDA10D2, bandwidth DC-25 MHz, 900–2600 nm spectral range, 5 kV/A transimpedence gain) connected to an electronic spectrum analyzer (ESA) (Signal Hound USB-SA44B, bandwitdh 1 Hz–4.4 GHz). A DC block capacitor with cut-off frequency < 3 Hz was used at the input of the ESA. The photodiode signal was additionally filtered by a 20 MHz low-pass filter to avoid saturation of the ESA at the pulse repetition rate. The full noise power spectrum was then recorded in multiple steps with resolution bandwidths adapted to the recorded frequency range. The chosen resolutions were: 1 Hz in the range 10 Hz–1 kHz, 10 Hz in the range 1–10 kHz, 100 Hz in the range 10 kHz–1 MHz, and 10 kHz above 1 MHz. 50 averages were taken in each section. The measured spectra are normalized by the corresponding noise-equivalent bandwidths to yield the mean electrical noise power spectrum $\langle \mathscr{P}_N(f) \rangle$, which is then related to the measured mean electrical DC power $\langle \mathscr{P}_{DC} \rangle$ to yield the

$RIN(f) = \langle \mathscr{P}_N(f) \rangle / \langle \mathscr{P}_{DC} \rangle$ and displayed in logarithmic units dBc/Hz. Since $\mathscr{P}_N \propto P_N^2$ (optical noise power) and $\mathscr{P}_{DC} \propto P_C^2$ (optical carrier power), the root mean square optical intensity fluctuations are given by $\sqrt{\int RIN(f)\mathrm{d}f}$ integrated over a given frequency range. This value is used in this manuscript when integrated RIN values are referenced.

Data availability

The raw data for the significant figures in this paper is available online at https://doi.org/10.7892/boris.136244.

Received: 12 September 2019; Accepted: 17 September 2020
Published online: 07 October 2020

References

1. Schliesser, A., Picque, N. & Hansch, T. W. Mid-infrared frequency combs. *Nat. Photon.* **6**, 440–449 (2012).
2. Muraviev, A. V., Smolski, V. O., Loparo, Z. E. & Vodopyanov, K. L. Massively parallel sensing of trace molecules and their isotopologues with broadband subharmonic mid-infrared frequency combs. *Nat. Photon.* **12**, 209–214 (2018).
3. Lee, K. F., Hensley, C. J., Schunemann, P. G. & Fermann, M. E. Midinfrared frequency comb by difference frequency of erbium and thulium fiber lasers in orientation-patterned gallium phosphide. *Opt. Express* **25**, 17411–17416 (2017).
4. Gaida, C. *et al.* High-power frequency comb at 2 μm wavelength emitted by a Tm-doped fiber laser system. *Opt. Lett.* **43**, 5178–5181 (2018).
5. Butler, T. P. *et al.* Watt-scale 50-MHz source of single-cycle waveform-stable pulses in the molecular fingerprint region. *Opt. Lett.* **44**, 1730–1733 (2019).
6. Gaida, C. *et al.* Ultrafast thulium fiber laser system emitting more than 1 kW of average power. *Opt. Lett.* **43**, 5853–5856 (2018).
7. Hemming, A., Simakov, N., Haub, J. & Carter, A. A review of recent progress in holmium-doped silica fibre sources. *Opt. Fiber Technol.* **20**, 621–630 (2014).
8. Li, Z. *et al.* Thulium-doped fiber amplifier for optical communications at 2 μm. *Opt. Express* **21**, 9289–9297 (2013).
9. Li, Z. *et al.* Extreme short wavelength operation (1.65–1.7 μm) of silica-based thulium-doped fiber amplifier. in *Optical Fiber Communication Conference*, Tu2C–1 (Optical Society of America, 2015).
10. Adler, F. & Diddams, S. A. High-power, hybrid Er:fiber/Tm:fiber frequency comb source in the 2 μm wavelength region. *Opt. Lett.* **37**, 1400–1402 (2012).
11. Kumkar, S. *et al.* Femtosecond coherent seeding of a broadband Tm: fiber amplifier by an Er: fiber system. *Opt. Lett.* **37**, 554–556 (2012).
12. Coluccelli, N., Cassinerio, M., Laporta, P. & Galzerano, G. Single-clad Tm–Ho: fiber amplifier for high-power sub-100-fs pulses around 1.9 μm. *Opt. Lett* **38**, 2757–2759 (2013).
13. Hoogland, H. *et al.* All-PM coherent 2.05 μm thulium/holmium fiber frequency comb source at 100 MHz with up to 0.5 W average power and pulse duration down to 135 fs. *Opt. Express* **21**, 31390–31394 (2013).
14. Coluccelli, N., Cassinerio, M., Gambetta, A., Laporta, P. & Galzerano, G. High-power frequency comb in the range of 2–2.15 μm based on a holmium fiber amplifier seeded by wavelength-shifted Raman solitons from an erbium-fiber laser. *Opt. Lett.* **39**, 1661–1664 (2014).
15. Tan, F., Shi, H., Sun, R., Wang, P. & Wang, P. 1 μj, sub-300 fs pulse generation from a compact thulium-doped chirped pulse amplifier seeded by Raman shifted erbium-doped fiber laser. *Opt. Express* **24**, 22461–22468 (2016).
16. Soboń, G. *et al.* All-in-fiber amplification and compression of coherent frequency-shifted solitons tunable in the 1800–2000 nm range. *Photon. Res.* **6**, 368–372 (2018).
17. Dudley, J. M., Genty, G. & Coen, S. Supercontinuum generation in photonic crystal fiber. *Rev. Mod. Phys.* **78**, 1135–1184 (2006).
18. Newbury, N., Washburn, B., Corwin, K. & Windeler, R. Noise amplification during supercontinuum generation in microstructure fiber. *Opt. Lett.* **28**, 944–946 (2003).
19. Corwin, K. L. *et al.* Fundamental noise limitations to supercontinuum generation in microstructure fiber. *Phys. Rev. Lett.* **90**, 113904 (2003).
20. Newbury, N. R. & Swann, W. C. Low-noise fiber-laser frequency combs (invited). *J. Opt. Soc. Am. B* **24**, 1756–1770 (2007).
21. Heuermann, T., Gaida, C., Gebhardt, M. & Limpert, J. Thulium-doped nonlinear fiber amplifier delivering 50 fs pulses at 20 W of average power. *Opt. Lett.* **43**, 4441–4444 (2018).
22. Nomura, Y. & Fuji, T. Generation of watt-class, sub-50 fs pulses through nonlinear spectral broadening within a thulium-doped fiber amplifier. *Opt. Express* **25**, 13691–13696 (2017).
23. Gaida, C. *et al.* Self-compression in a solid fiber to 24 MW peak power with few-cycle pulses at 2 μm wavelength. *Opt. Lett.* **40**, 5160–5163 (2015).
24. Heidt, A. M. Pulse preserving flat-top supercontinuum generation in all-normal dispersion photonic crystal fibers. *J. Opt. Soc. Am. B* **27**, 550–559 (2010).
25. Heidt, A. M., Hartung, A. & Bartelt, H. *The Supercontinuum Laser Source: The Ultimate White Light, Chap. Generation of Ultrashort and Coherent Supercontinuum Light Pulses in All-Normal Dispersion Fibers*, 247–280 (Springer, New York, 2016).
26. Heidt, A. M., Feehan, J. S., Price, J. H. V. & Feurer, T. Limits of coherent supercontinuum generation in normal dispersion fibers. *J. Opt. Soc. Am. B* **34**, 764–775 (2017).
27. Rothhardt, J. *et al.* High stability soliton frequency-shifting mechanisms for laser synchronization applications. *J. Opt. Soc. Am. B* **29**, 1257–1262 (2012).
28. Shreesha Rao, D. S. *et al.* Ultra-low-noise supercontinuum generation with a flat near-zero normal dispersion fiber. *Opt. Lett.* **44**, 2216–2219 (2019).
29. Genier, E. *et al.* Amplitude noise and coherence degradation of femtosecond supercontinuum generation in all-normal-dispersion fibers. *J. Opt. Soc. Am. B* **36**, A161–A167 (2019).
30. Heidt, A. M. *et al.* High quality sub-two cycle pulses from compression of supercontinuum generated in all-normal dispersion photonic crystal fiber. *Opt. Express* **19**, 13873–13879 (2011).
31. Demmler, S. *et al.* Generation of high quality, 1.3 cycle pulses by active phase control of an octave spanning supercontinuum. *Opt. Express* **19**, 20151–20158 (2011).
32. Rothhardt, J., Demmler, S., Hädrich, S., Limpert, J. & Tünnermann, A. Octave-spanning OPCPA system delivering CEP-stable few-cycle pulses and 22 W of average power at 1 MHz repetition rate. *Opt. Express* **20**, 10870–10878 (2012).
33. Rothhardt, J., Hädrich, S., Delagnes, J., Cormier, E. & Limpert, J. High average power near-infrared few-cycle lasers. *Laser Photon. Rev.*https://doi.org/10.1002/lpor.201700043 *(2017).*
34. Klimczak, M., Siwicki, B., Heidt, A. & Buczyński, R. Coherent supercontinuum generation in soft glass photonic crystal fibers. *Photon. Res.* **5**, 710–727 (2017).
35. Heidt, A. M., Spangenberg, D.-M., Brügmann, M., Rohwer, E. G. & Feurer, T. Improved retrieval of complex supercontinuum pulses from XFROG traces using a ptychographic algorithm. *Opt. Lett.* **41**, 4903–4906 (2016).

36. Klimczak, M. *et al.* Coherent supercontinuum bandwidth limitations under femtosecond pumping at 2 μm in all-solid soft glass photonic crystal fibers. *Opt. Express* **24**, 29406–29416 (2016).
37. Ciąćka, P., Rampur, A., Heidt, A., Feurer, T. & Klimczak, M. Dispersion measurement of ultra-high numerical aperture fibers covering thulium, holmium, and erbium emission wavelengths. *J. Opt. Soc. Am. B* **35**, 1301–1307 (2018).
38. Tang, Y., Chong, A. & Wise, F. W. Generation of 8 nJ pulses from a normal-dispersion thulium fiber laser. *Opt. Lett.* **40**, 2361–2364 (2015).
39. Chen, S. *et al.* Tm: Ho co-doped single mode optical fibre laser pumped by a 1600 nm Er fibre laser. *Opt. Commun.* **281**, 2567–2571 (2008).
40. Liu, Y. *et al.* Suppressing short-term polarization noise and related spectral decoherence in all-normal dispersion fiber supercontinuum generation. *J. Lightwave Technol.* **33**, 1814–1820 (2015).
41. Gonzalo, I. B., Engelsholm, R. D., Sørensen, M. P. & Bang, O. Polarization noise places severe constraints on coherence of all-normal dispersion femtosecond supercontinuum generation. *Sci. Rep.* **8**, 6579 (2018).
42. Wabnitz, S. Modulational polarization instability of light in a nonlinear birefringent dispersive medium. *Phys. Rev. A* **38**, 2018 (1988).
43. Dobrakowski, D. *et al.* Development of highly nonlinear polarization-maintaining fibers with normal dispersion across entire transmission window. *J. Opt.* **21**, 015504 (2019).
44. Tarnowski, K., Martynkien, T., Mergo, P., Sotor, J. & Soboń, G. Compact all-fiber source of coherent linearly polarized octave-spanning supercontinuum based on normal dispersion silica fiber. *Sci. Rep.* **9**, 1–8 (2019).
45. Rampur, A. *et al.* Ultra low-noise coherent supercontinuum amplification and compression below 100 fs in an all-fiber polarization-maintaining thulium fiber amplifier. *Opt. Express* **27**, 35041–35051 (2019).
46. Scott, R. P., Langrock, C. & Kolner, B. H. High-dynamic-range laser amplitude and phase noise measurement techniques. *IEEE J. Sel. Top. Quant. Electron.* **7**, 641–655 (2001).

Acknowledgements

Swiss National Science Foundation (SNSF) (PCEFP2-181222, NCCR MUST). Fundacja na rzecz Nauki Polskiej (FNP) (First TEAM/2016-1/1). J. M. H. acknowledges support by the Carnegie Corporation of New York under its "Next Generation of Acedemics in Africa" project, A.R. acknowledges a Fellowship by the Schlumberger Foundation (Faculty for the Future).

Author contributions

A.H , M.K. and T.F. conceived the study. M.K. designed and supplied the nonlinear fiber. A.H., J.M.H., M.R. and A.R. designed and built the Tm/Ho amplifier. D.S., A.R. and A.H. performed RIN measurements and corresponding data analysis. A.R. and M.K. performed fiber dispersion measurements. A.H. and J.M.H. set up autocorrelation measurements and analysis. A.R. and M.K. performed the spectrogram measurement of the SC pulse, A.H. the analysis. All Authors contributed to scientific interpretation of results, writing, and editing of the article.

Competing interests

The authors declare no competing interests.

Additional information

Correspondence and requests for materials should be addressed to A.M.H.

Reprints and permissions information is available at www.nature.com/reprints.

Publisher's note Springer Nature remains neutral with regard to jurisdictional claims in published maps and institutional affiliations.